

## Numerical analysis of dynamic debonding under anti-plane shear loading

PHILIPPE H. GEUBELLE\* and M. SCOT BREITENFELD

*Department of Aeronautical and Astronautical Engineering, University of Illinois at Urbana–Champaign, Urbana, IL 61801, U.S.A.*

Received 4 December 1996; accepted in revised form 2 July 1997

**Abstract.** We present an efficient numerical scheme specially developed to simulate a wide variety of dynamic debonding problems under anti-plane shear loading conditions. The algorithm is based on an exact spectral representation of the elastodynamic relations between the interface stresses and displacements. It involves an explicit time stepping scheme with, for each time step, the use of FFT to link the spatial and spectral domains, and the computation of a convolution over the past displacement or velocity history. Two versions of the spectral algorithm are presented: in the first one, the elastodynamic response of each half space is investigated separately before the two solutions are linked with the aid of the interface continuity conditions. In the second approach, the interface conditions and the modulus mismatch are combined in a single bimaterial elastodynamic relation. Various problems involving stationary or rapidly moving interfacial cracks are investigated and contrasted with existing analytical results.

**Key words:** dynamic fracture, spectral method, interface, boundary integral method.

### 1. Introduction

Often considered as the weak points of engineering structures, interfaces have been the focus of extensive research to better understand and characterize the mechanics of their failure. However, due to the complexity of the relations involved, most investigations have been performed for the static case, and the dynamic fracture of bimaterial interfaces has only received limited attention despite the existence of various interesting phenomena and issues which need to be addressed. The first issue is the appearance of a zone in the vicinity of the crack tip in which the crack faces are predicted to overlap and the stresses show oscillations. This undesirable result which appears in both static and dynamic situations has been shown to be associated with the existence of a complex singularity characterizing the near-tip stress and strain fields in the in-plane cases (Williams, 1959). This peculiarity does not however arise in the 2D anti-plane shear situation where a more conventional real singularity is predicted.

Various approaches have been suggested to remedy this problem in the static case, including the introduction of a frictionless contact (Comninou, 1977), the recourse to finite elastostatics (Knowles and Sternberg, 1983; Geubelle, 1995), or the adoption of smoothly varying material properties through the interface (Delale and Erdogan, 1988). However, since the size of the interpenetration region is very small in most static cases, its effects are usually neglected by using the concept of a ‘contact zone’ (Rice, 1988) outside of which the linearly elastic solution is expected to hold. This practical approach has now been generally adopted by the fracture mechanics community to solve a wide range of static interfacial fracture problems.

---

\* Corresponding author.

In dynamic debonding problems, however, this approach might not be adequate since the imaginary part of the near-tip singularity (commonly referred to as the oscillatory index  $\varepsilon$ ), and thereby the size of the interpenetration zone, increase drastically with the crack velocity; especially as the crack speed approaches the slowest Rayleigh wave speed (Yang et al. 1991).

The issue of crack face interpenetration and contact is not, however, the only interesting aspect of dynamic interfacial fracture mechanics. Recent experiments (Tippur and Rosakis, 1991; Lambros and Rosakis, 1995), have demonstrated the existence of unexpectedly fast subsonic and even transonic cracks propagating along a PMMA/Al interface: the crack speed was shown to approach and even exceed the Rayleigh wave speed of the PMMA. These observations have motivated a series of analytical studies pertaining to the structure of the near-tip fields under dynamic debonding. Yang et al. (1991) have used the Stroh formulation to investigate the subsonic steady-state motion of interfacial cracks under in-plane and anti-plane shear loading conditions in isotropic and anisotropic material combinations. Yu and Yang have discussed the 2D transonic anti-plane shear (Yu and Yang, 1994) and in-plane (Yu and Yang, 1995) problems. Liu et al. (1993, 1995) have studied the structure of the near-tip fields under steady-state and transient conditions in both the subsonic and transonic cases. These various asymptotic investigations complete earlier work summarized by Atkinson (1977).

Unlike their homogeneous counterparts, most bimaterial problems are characterized by an intrinsic combination of the tensile (mode I) and shear (mode II) fracture modes. This complex interaction between normal and tangential stress and displacement components along the fracture plane is expected to yield some unfamiliar phenomena which extend even outside the framework of dynamic debonding. Among these is the possible onset of instability associated with the frictional contact of two dissimilar materials: in a recent 2D analytical investigation, Adams (1995) has shown that, under certain conditions, the relative motion of two planar surfaces can generate self-excited oscillations of increasing amplitudes even if the contact is characterized by a Coulomb friction law with a constant coefficient. The relative motion of materials of different properties has also been examined by Andrews and Ben-Zion (1997) who studied the evolution of a wrinkle-like slip pulse between dissimilar crustal blocks under plane strain conditions, and its influence on the normal tractions acting on the interfacial plane.

The richness of the topics associated with dynamic debonding and with the relative frictional motion of dissimilar planar media motivates the need for additional studies. However, due to the complexity of the elastodynamic relations involved in interface fracture problems, analytical solutions are limited to simple 2D geometries (such as a semi-infinite interfacial crack), steady-state conditions and/or imposed crack motion. Numerical schemes are therefore needed to investigate the phenomena associated with fully 3D bimaterial geometries, time-dependent loading conditions and/or spontaneous crack propagation and to allow the introduction of more realistic models needed to capture the interfacial failure process and/or the frictional contact between the two components.

A few numerical schemes have already been used in interfacial dynamic fracture problems. Day (1991) and Andrews and Ben-Zion (1997) have used the finite difference method to investigate various geophysically related bimaterial problems. Lo et al. (1994) have studied dynamic debonding in a plate using a conventional finite element scheme. Xu and Needleman (1995, 1996) have introduced a special volumetric/cohesive finite element scheme allowing for the spontaneous generation of new surfaces along and off an interface.

The objective of this series of two papers is to develop a novel efficient numerical scheme specially designed to investigate a wide range of 2D and 3D dynamic bimaterial problems

such as the dynamic loading of interfacial cracks, the spontaneous propagation of fast cracks and the relative motion of two elastic media.

The proposed numerical method described hereafter is inspired from the spectral scheme recently developed by Geubelle and Rice (1995) to study various issues associated with 3D dynamic fracture problems in homogeneous isotropic linearly elastic media. The scheme, which is based on a spectral representation of the elastodynamic relations between the traction stresses and the displacement discontinuities along the fracture plane, has been shown to provide a unique tool to study a wide range of dynamic rupture related issues with very high precision.

In this preliminary paper, the simpler 2D anti-plane shear problem is presented to illustrate the major differences between the homogeneous and bimaterial situations. The ability of the numerical scheme to capture complex wave interactions and evolving near-tip singularity is demonstrated. As mentioned earlier, the issues associated with the presence of contact or interpenetration zones and with the intrinsic mode-mixity do not arise in the context of anti-plane shear loading. These issues will be discussed in the more challenging 2D in-plane and fully 3D bimaterial cases described in the sequel (Breitenfeld and Geubelle, 1997), together with various unresolved issues associated with limiting spontaneous debonding speeds, transonic crack propagation and dynamic failure of heterogeneous bonds.

This first paper is organized as follows: the two basic formulations of the bimaterial spectral scheme are described in the second section, and are contrasted with the homogeneous case. Then, the classical problem of a non-moving finite crack subjected to a sudden uniform anti-plane shear load is investigated to illustrate the ability of the numerical scheme to capture complex wave interactions along the fracture surfaces and along the interface. Finally, various issues associated with propagating fast cracks are discussed; in particular, the velocity dependence of the near-tip singularity in the transonic range, and the spontaneous motion of interfacial cracks. A comparison with analytical solutions is provided when available.

## 2. Presentation of the spectral scheme

The failure mechanics of interfaces under anti-plane shear conditions is not very different from its homogeneous counterpart. Just like in the homogeneous situation, this particular fracture mode can be studied separately from the other in-plane modes, and is expected to yield (at least in the subsonic case) a near-tip field structure similar to that of a mode III crack propagating in a homogeneous body. This similarity can be found in the derivation of the spectral scheme: the initial steps leading to the spectral formulation of the bimaterial anti-plane shear problem are similar to those used by Perrin et al. (1994) and Geubelle and Rice (1995) in the homogeneous situation. The major difference between homogeneous and bimaterial cases pertains to how the absence of symmetry in the mechanical response of the upper and lower half spaces is accounted for in the spectral formulation. Two basic approaches can be considered: the first approach, referred to as the *independent spectral formulation* in the remainder of this paper, consists of modeling the elastodynamic responses in the two half spaces through two independent ‘homogeneous’ integral equations before joining them with the appropriate boundary conditions along the interface. The second approach, referred to hereafter as the *combined spectral formulation*, incorporates the elastodynamic response of both half spaces and the interface conditions into a single ‘bimaterial’ integral equation involving the displacement discontinuity (or slip) observed on the fracture plane. Although these two approaches have the same underlying principle and often yield similar results (espe-

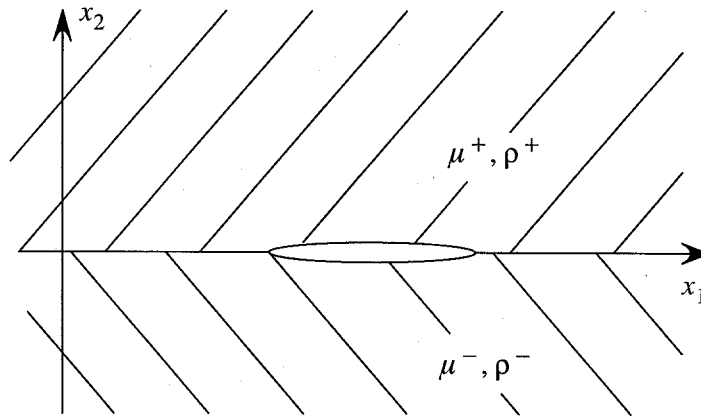


Figure 1. Geometry of the mode III interface fracture problem.

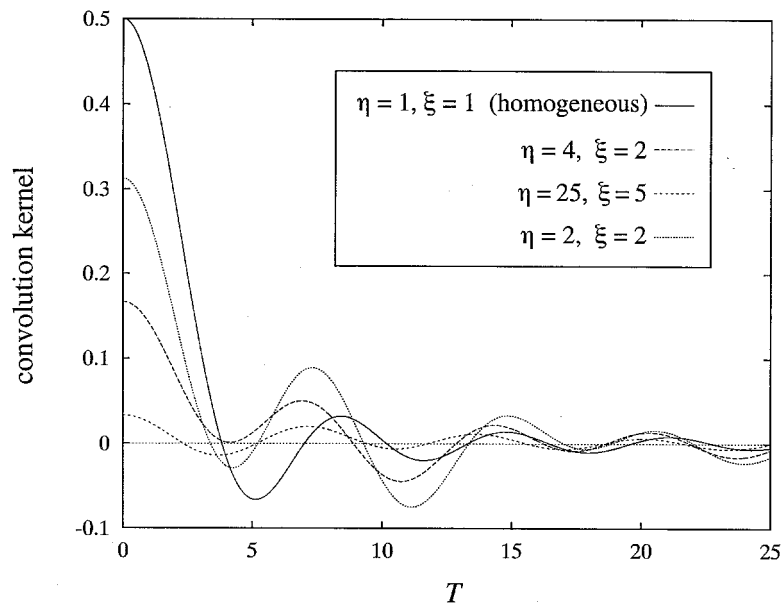


Figure 2. Convolution kernel for the mode III combined spectral formulation (7) for various values of  $\eta = \mu^+/\mu^-$  and  $\xi = c_s^+/c_s^-$ .

cially in the mode III case considered in this paper), they differ slightly with respect to their numerical implementation. Furthermore, the independent and combined spectral formulations present quite different stability characteristics in the in-plane (modes I/II) situation as shown in the sequel (Breitenfeld and Geubelle, 1997).

The main objectives of this section are to describe the main steps leading to the derivation of the two spectral formulations in the bimaterial mode III case, to discuss their respective numerical implementation, and to comment on their merits and disadvantages.

Consider the 2D interfacial fracture problem represented in Figure 1. Quantities associated with the upper and lower materials are denoted by the superscripts ‘+’ and ‘-’, respectively<sup>1</sup>.

<sup>1</sup> For clarity of the notations, the superscripts are included only when required.

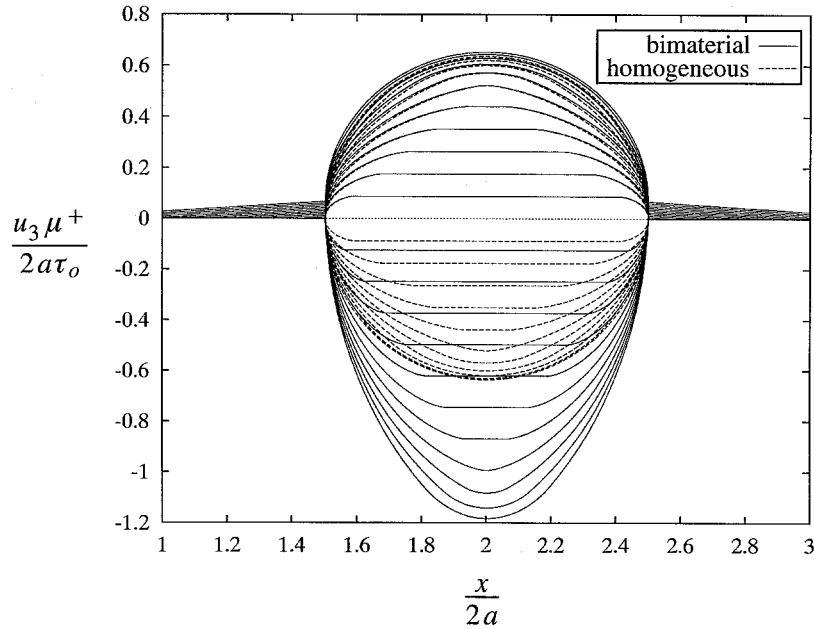


Figure 3. Sudden uniform anti-plane loading of a non-propagating crack of length  $2a$  showing the interaction of the shear waves emanating from the crack tips and propagating along the upper and lower crack faces. The curves are separated by 100 time steps.

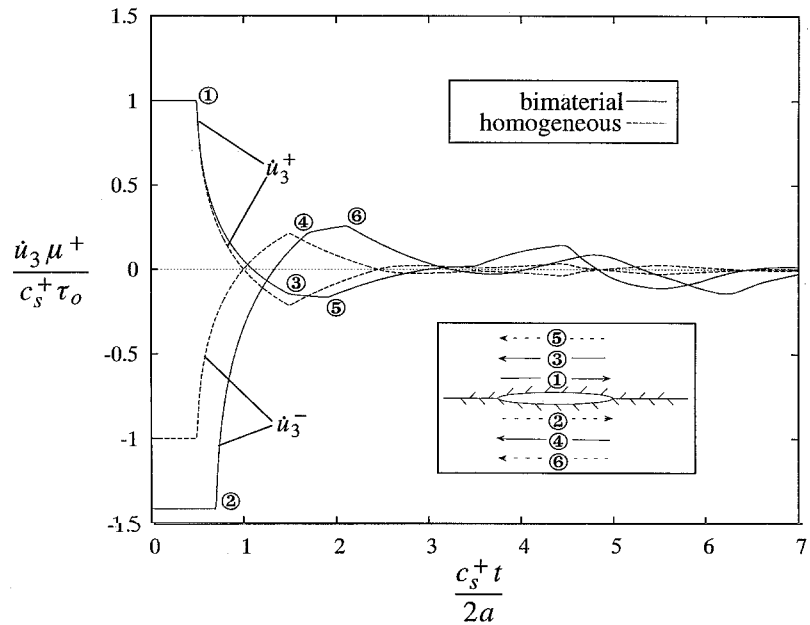


Figure 4. Evolution of the velocity  $\dot{u}_3$  at the center of the top and bottom faces for a stationary crack under uniform sudden anti-plane shear loading. The circled numbers denote the passage of various waves originating at the crack tips, as illustrated in the insert.

Within the framework of anti-plane shear,  $u_3(x_1, x_2, t)$  is the only non-zero displacement component and satisfies the scalar wave equation

$$c_s^2 \nabla^2 u_3 = \ddot{u}_3, \tag{1}$$

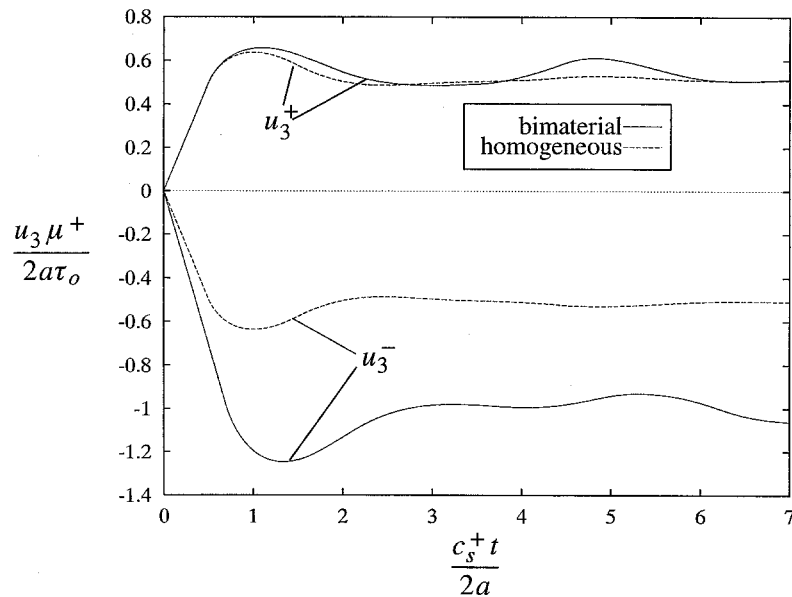


Figure 5. Evolution of the displacement  $u_3$  at the center of the top and bottom faces for a stationary crack under uniform sudden anti-plane shear loading  $\tau_0$ .

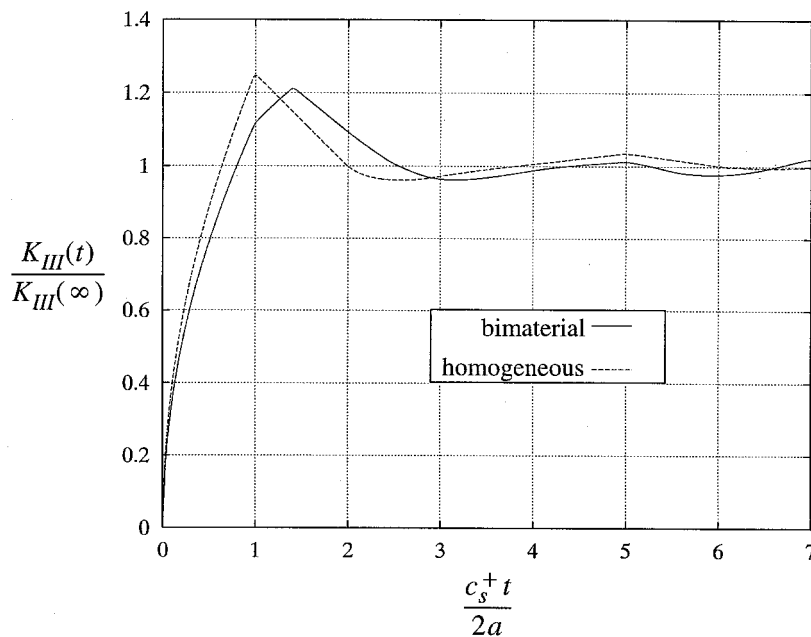


Figure 6. Evolution of the dynamic stress intensity factor  $K_{III}$  (normalized by its static limit) for a suddenly uniformly loaded mode III crack.

where the dot denotes differentiation with respect to time;  $c_s = \sqrt{\mu/\rho}$  is the shear wave speed;  $\mu$  and  $\rho$  are the shear modulus and density, respectively.

The spectral formulation is a special form of the boundary integral equation and therefore involves the displacement and the traction stress along the fracture plane ( $x_2 = 0$ ). More

precisely, it relates their respective time-dependent Fourier coefficients defined by

$$\begin{aligned} u_3(x_1, x_2 = 0^\pm, t) &= u_3^\pm(x_1, t) = U_3^\pm(t; q) e^{iqx_1}, \\ \sigma_{23}(x_1, x_2 = 0, t) &= \tau_3(x_1, t) = T_3(t; q) e^{iqx_1}. \end{aligned}$$

As described in Geubelle and Rice (1995), Equation (20), the Fourier coefficients of the elastodynamic stress and displacement fields satisfying (1) are related in the Laplace domain by

$$\widehat{T}_3(p; q) = \mp \mu^\pm |q| \alpha_s^\pm \widehat{U}_3^\pm(p; q), \quad (2)$$

where  $\widehat{f}(p)$  denotes the Laplace transform of  $f(t)$  and

$$\alpha_s = \sqrt{1 + \frac{p^2}{|q|^2 c_s^2}}.$$

Equation (2) serves as the foundation of both the independent and combined spectral formulations.

### 2.1. INDEPENDENT FORMULATION

In this approach, we examine the elastodynamic response of the two half spaces separately. We start by extracting the instantaneous response of the two half-spaces

$$\tau_{3\text{inst}}(x_1, t) = \mp \frac{\mu^\pm}{c_s^\pm} \dot{u}_3^\pm(x_1, t), \quad (3)$$

and rewrite (2) as

$$\widehat{T}_3(p; q) = \pm \frac{\mu^\pm}{c_s^\pm} p \widehat{U}_3^\pm(p; q) \mp \mu^\pm |q| \left( \alpha_s^\pm - \frac{p}{|q| c_s^\pm} \right) \widehat{U}_3^\pm(p; q). \quad (4)$$

Back in the time domain, (4) yields

$$\tau_3(x_1, t) = \tau_3^0(x_1, t) \mp \frac{\mu^\pm}{c_s^\pm} \dot{u}_3^\pm(x_1, t) + f_3^\pm(x_1, t), \quad (5)$$

where the externally applied anti-plane shear traction stress  $\tau_3^0(x_1, t)$  associated, for example, with the arrival of a plane wave has been added to the interface stress, and where  $f_3^\pm(x_1, t)$  represents the convolution term corresponding to the last term of (4). This convolution term is expressed in the Fourier domain as

$$f_3^\pm(x_1, t) = F_3^\pm(t; q) e^{iqx_1}, \quad (6)$$

where the Fourier coefficient  $F_3^\pm(t; q)$  is given by the convolution integral

$$F_3^\pm(t; q) = \mp \mu^\pm |q| \int_0^t C_{\text{III}}^{\text{in}}(|q| c_s^\pm(t - t')) U_3^\pm(t'; q) |q| c_s^\pm dt'. \quad (7)$$

The convolution kernel of the independent formulation  $C_{\text{III}}^{\text{in}}(T)$  is given by

$$C_{\text{III}}^{\text{in}}(T) = \frac{J_1(T)}{T}, \quad (8)$$

where  $J_1(T)$  is the Bessel function. The convolution kernel is represented by the solid curve in Figure 2. Relations (5) to (8) constitute the basic elastodynamic equations for the independent spectral formulation. As described in (Geubelle and Rice, 1995), the convolution term given by (7) can be integrated by parts and rewritten as a convolution on the past velocity history instead of the displacement history. The remaining equations and the numerical implementation will be described at the end of this section.

## 2.2. COMBINED FORMULATION

In this approach, the elastodynamic solutions on the two half spaces are combined by introducing two auxiliary quantities

$$\begin{aligned} \zeta(x_1, t) &= u_3^+(x_1, t) + u_3^-(x_1, t) = S(t; q) e^{iqx_1}, \\ \delta(x_1, t) &= u_3^+(x_1, t) - u_3^-(x_1, t) = D(t; q) e^{iqx_1}. \end{aligned} \quad (9)$$

After inversion of the latter relations, (2) can be rewritten as

$$\hat{T}_3(p; q) = -\frac{\mu^+ |q| \alpha_s^+}{2} (\hat{D}(p; q) + \hat{S}(p; q)) = \frac{\mu^- |q| \alpha_s^-}{2} (\hat{S}(p; q) - \hat{D}(p; q)). \quad (10)$$

Defining non-dimensional mismatch ratios

$$\eta = \frac{\mu^+}{\mu^-}, \quad \xi = \frac{c_s^+}{c_s^-}, \quad (11)$$

and eliminating the auxiliary quantity  $S(t; q)$ , we can rewrite (10) as

$$\hat{T}_3(p; q) = -\mu^+ |q| \alpha_s^+ \left( \frac{1}{1 + \eta \sqrt{\frac{1+s^2}{1+\xi^2 s^2}}} \right) \hat{D}(p; q),$$

with  $s = p/|q|c_s^+$ .

We now extract the instantaneous response derived from (3) as

$$T_{3\text{inst}}(t; q) = -\frac{\mu^+}{c_s^+} \frac{1}{1 + \frac{\eta}{\xi}} \dot{D}(t; q)$$

to obtain

$$\begin{aligned} \hat{T}_3(p; q) &= -\frac{\mu^+}{c_s^+} \frac{1}{1 + \frac{\eta}{\xi}} p \hat{D}(p; q) \\ &\quad - \frac{\mu^+ |q|}{2} \left\{ \alpha_s^+ \frac{2}{1 + \eta \sqrt{\frac{1+s^2}{1+\xi^2 s^2}}} - \frac{2s}{\left(1 + \frac{\eta}{\xi}\right)} \right\} \hat{D}(p; q). \end{aligned} \quad (12)$$

In the time domain, the relation between the interface stress  $\tau_3(x_1, t)$  and the resulting crack opening displacement  $\delta(x_1, t)$  is thus

$$\tau_3(x_1, t) = \tau_3^0(x_1, t) - \frac{\mu^+}{c_s^+} \frac{1}{1 + \frac{\eta}{\xi}} \dot{\delta}(x_1, t) + f_3^c(x_1, t), \quad (13)$$

where the Fourier coefficient of the convolution term  $f_3^c(x_1, t)$  is now

$$F_3^c(t; q) = -\frac{1}{2} u^+ |q| \int_{-\infty}^t C_{\text{III}}^c(|q| c_s^+ t'; \eta, \xi) D(t - t'; q) |q| c_s^+ dt'. \quad (14)$$

The convolution kernel for the combined spectral formulation  $C_{\text{III}}^c(T; \eta, \xi)$  is given by the inverse Laplace transform of the term in curly brackets in (12)

$$C_{\text{III}}^c(T; \eta, \xi) = \mathcal{L}^{-1} \left\{ \frac{2\sqrt{1+s^2}}{1 + \eta\sqrt{\frac{1+s^2}{1+\xi^2 s^2}}} - \frac{2s}{1 + \frac{\eta}{\xi}} \right\}. \quad (15)$$

It has been inverted numerically and is presented in Figure 2 for various values of  $\eta$  and  $\xi$  defined in (11). The initial value of the kernel is

$$C_{\text{III}}^c(T = 0; \eta, \xi) = \frac{\eta + \xi^3}{\xi^3 + 2\xi^2\eta + \xi\eta^2}.$$

Note that, as expected, we retrieve  $C_{\text{III}}^c(T; 1, 1) = J_1(T)/T$  in the homogeneous limit. Relations (13)–(15) constitute the fundamental elastodynamic equations of the combined approach.

### 2.3. NUMERICAL IMPLEMENTATION AND COMPARISON BETWEEN THE TWO APPROACHES

The elastodynamic relations (5) and (7) (or (13) and (14)) are completed by a constitutive relation characterizing the failure process (for dynamic debonding simulations) and/or the frictional contact between the two half spaces. In its most general form, the constitutive law is expressed as

$$\tau_{\text{strength}} = f(\delta, \dot{\delta}, x_1, t), \quad (16)$$

where the slip  $\delta(x_1, t)$  had been defined in (9).

The numerical implementation of the two interfacial spectral schemes is similar to its homogeneous counterpart detailed in Morrissey and Geubelle (1997): it is based on the discretization of a portion  $X$  of the interfacial plane by a uniform grid of  $N$  spacings, on implementing the FFT algorithm (based on the grid points) to efficiently perform the transition between spatial and spectral domains, and on an explicit time integration introduced to compute the displacement distribution from the velocity components obtained in (5) (or (13)).

The only difference regarding the numerical implementation pertains to the way the absence of symmetry across the interface is incorporated in the formulation. To illustrate this fact, let us consider the case of the simple rate-independent linear cohesive law used in (Geubelle and

Rice, 1995) in which the interfacial strength  $\tau_{\text{strength}}$  decreases linearly with the slip  $\delta$  from an 'intact' value  $\tau_c$  at  $\delta = 0$  to zero when a critical slip  $\delta_c$  is reached, beyond which complete failure is achieved.

Since the material asymmetry is intrinsically included in the elastodynamic relations (13) and (14), the implementation of the combined approach is straightforward

$$\frac{1}{c_s^\pm} \dot{\delta}(x_1, t) = \begin{cases} \frac{1}{\mu^+} \left( 1 + \frac{\eta}{\xi} \right) (\tau_3^0(x_1, t) + f_3^c(x_1, t) - \tau_{\text{strength}}(x_1, t)), \\ \text{if } \tau_{\text{strength}} < |\tau_3^0 + f_3^c|, \\ 0, \text{ otherwise.} \end{cases} \quad (17)$$

In the independent approach, where the motions of each half space surface are described independently by (5), continuity of the displacement  $u_3$  and tractions  $\tau_3$  along the interface can be shown to yield

$$\begin{cases} \dot{u}_3^+ = \dot{u}_3^- = \frac{c_s^+}{\mu^+} \left( \frac{f_3^+ - f_3^-}{1 + \frac{\xi}{\eta}} \right), & \text{if } (\tau_{\text{strength}} > \tau_{\text{interface}}), \\ \dot{u}_3^\pm = c_s^\pm \left( \frac{\tau_3^0 + f_3^\pm - \tau_{\text{strength}}}{\mu^\pm} \right), & \text{otherwise,} \end{cases} \quad (18)$$

where  $\tau_{\text{interface}}$  is the traction stress appearing on the interface in the absence of failure and is given by

$$\tau_{\text{interface}} = \tau_3^0 + \frac{\frac{\xi}{\eta} f_3^+ + f_3^-}{1 + \frac{\xi}{\eta}}.$$

Relations (17) and (18) emphasize the differences between the independent and combined approaches. The main advantages of the latter are the simplicity of its implementation (since only the displacement discontinuity  $\delta$  must be accounted for) and its efficiency as only one convolution integral has to be computed. The independent approach however has a much simpler convolution kernel and also provides, through (18a), the motion of the interface in the uncracked region under the effect of the elastic waves traveling at different speeds in the two adjacent half spaces. In the anti-plane shear case, the two methods provide identical results for both the interface stress and displacement discontinuity. The stability characteristics are also similar, and the time step  $\Delta t$  can be typically chosen as large as

$$\beta = \frac{\max(c_s^+, c_s^-) \Delta t}{\Delta x} = \frac{1}{2},$$

i.e., it takes 2 time steps for the fastest wave to travel one grid spacing  $\Delta x = X/N$ . This similarity of the two approaches in both accuracy and stability does not however persist in the more challenging in-plane (modes I, II) case described in the sequel (Breitenfeld and Geubelle, 1997).

In the present two-dimensional anti-plane shear bimaterial case, the additional computational effort associated with the double convolution characterizing the independent spectral

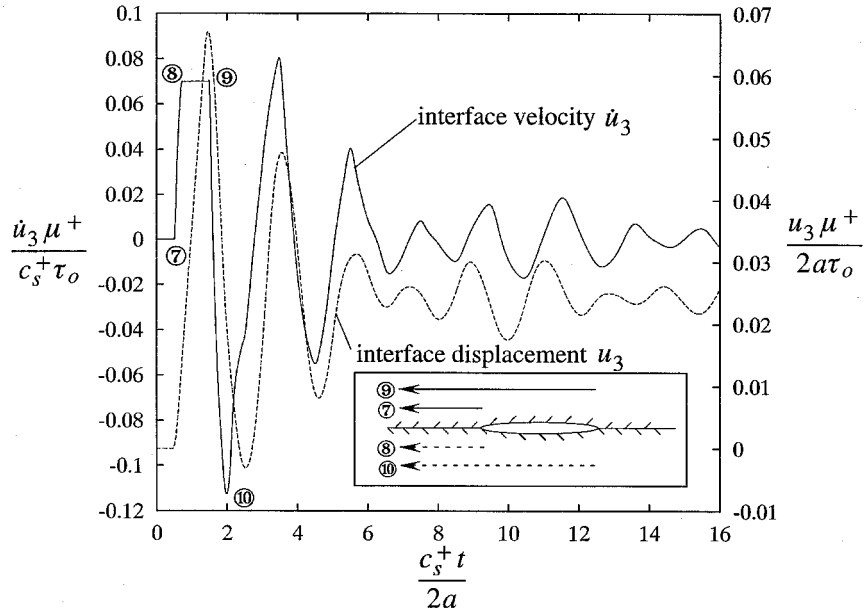


Figure 7. Velocity  $\dot{u}_3$  and displacement  $u_3$  of the interface at a distance  $a/8$  from the left tip of a center crack under sudden uniform anti-plane shear load.

scheme (5)–(8) does not constitute a major obstacle, and, since it provides additional information regarding the motion of the interface, this scheme will be used in the remainder of this paper.

In the next section, the classical problem of a finite-size non-propagating interfacial crack subjected to a sudden uniform anti-plane shear loading is presented to illustrate how precisely the spectral scheme described above can capture the complex wave interactions characterizing bimaterial elastodynamic problems.

### 3. Non-propagating interfacial crack under sudden uniform mode III loading

Let  $X$  denote the discretized portion of the interfacial plane, and let  $2a = X/4$  be the length of the pre-existing crack located at the center of the discretized domain, on which a uniform grid of 1024 elements is defined. The material properties are chosen such that  $\mu^+/\mu^- = 2$  and  $\rho^+/\rho^- = 1$  (resulting in  $c_s^+/c_s^- = \sqrt{2}$ ). The crack is suddenly subjected to a uniformly distributed anti-shear load  $\tau_0$  and is prevented from extending by applying a very high strength in the uncracked region with the motion of the interface therefore given by (18a). In the cracked portion of the domain, the strength is equal to zero and the motion of the crack faces is described by (18b). The time step  $\Delta t$  used in the explicit time integration scheme is chosen as  $\Delta x/2c_s^+$ .

The evolution of the deformed crack shape for the first 1100 time steps is presented in Figure 3. The homogeneous problem is also shown (dashed curves) for comparison. The simulation clearly shows the different speeds at which the information propagates along the fracture surfaces in the two materials, and how this difference affects the motion of the uncracked portion of the interface (which remains motionless in the homogeneous case).

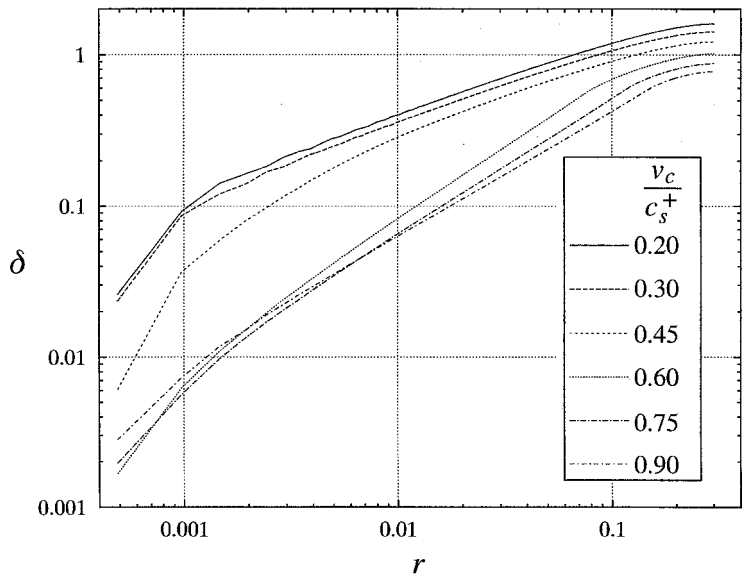


Figure 8. Spatial variation of the crack opening displacement in the vicinity of the crack tip for various values of imposed crack velocity  $c_s^+/c_s^- = \sqrt{2}$ .

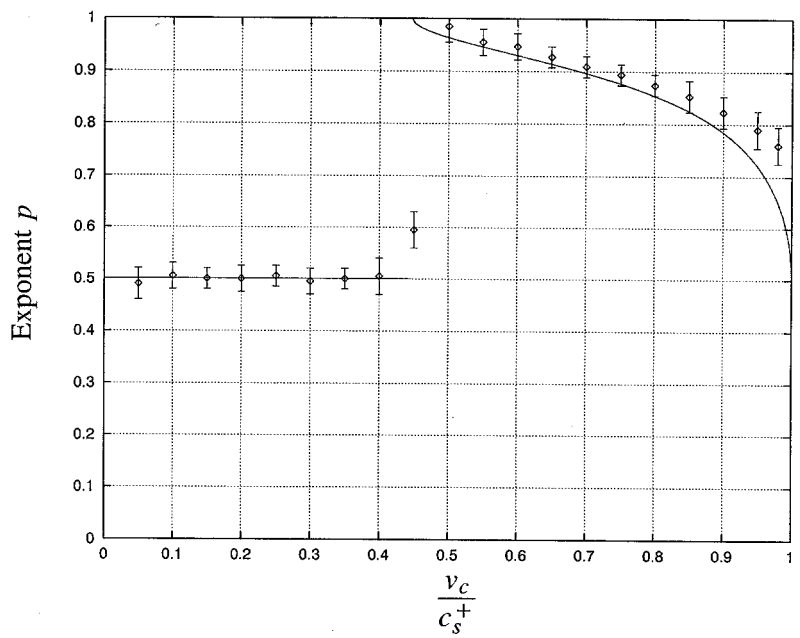


Figure 9. Effect of the imposed crack velocity on the exponent  $p$  characterizing the spatial variation of the crack opening displacement in the vicinity of the moving crack tip. The analytical solution is denoted by the solid curve and the symbols represent the numerical values. The error bars are associated with the imprecision of the fitting of the curves in Figure 8.

This fact is further illustrated in Figures 4 and 5 which present the evolution of the velocity  $\dot{u}_3$  and displacement  $u_3$  for the center points of the two crack faces, respectively. The circled numbers in Figure 4 indicate the arrival of the first series of elastic waves originating (or

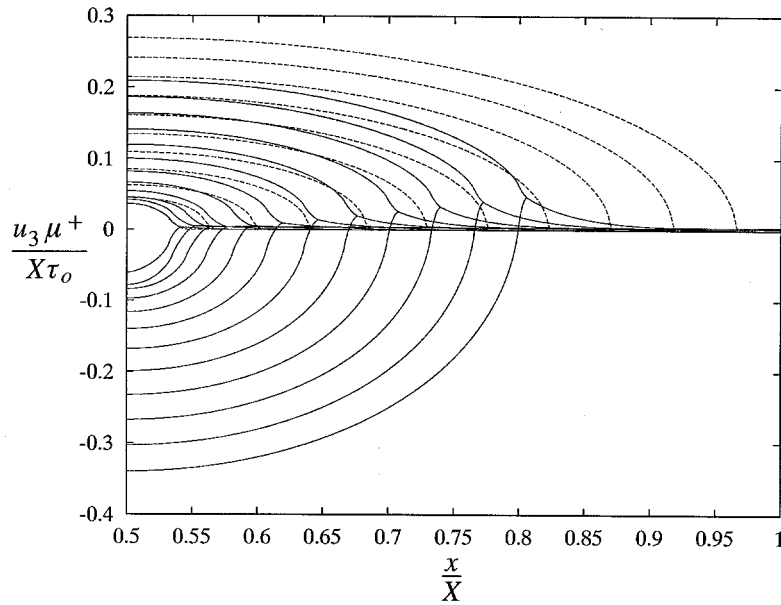


Figure 10. Evolution of the deformed shape of a spontaneously expanding mode III crack, for the homogeneous case and bimaterial case with  $\mu^+/\mu^- = 2$ . The time spacing between each curve corresponds to 200 time steps.

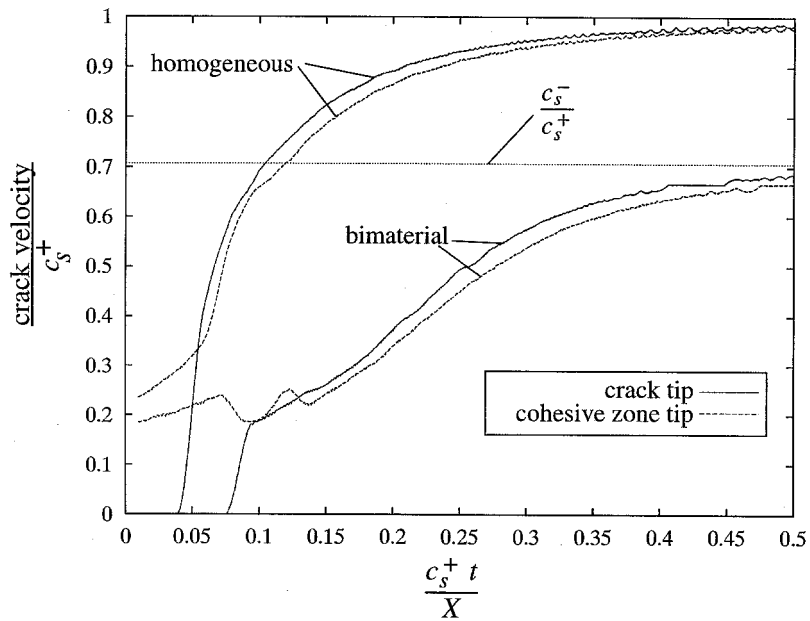


Figure 11. Time dependence of the velocities of the crack tip and of the Dugdale cohesive zone leading edge for the homogeneous and bimaterial spontaneous crack propagation problem presented in Figure 10. The horizontal dotted curve indicates the slowest shear wave speed for the bimaterial case.

reflecting) from the crack tips. The propagation paths of the waves are shown schematically in the insert of Figure 4. As was noticed experimentally by Lambros and Rosakis (1995), transient effects are more severe in the bimaterial situation than in the homogeneous one. This

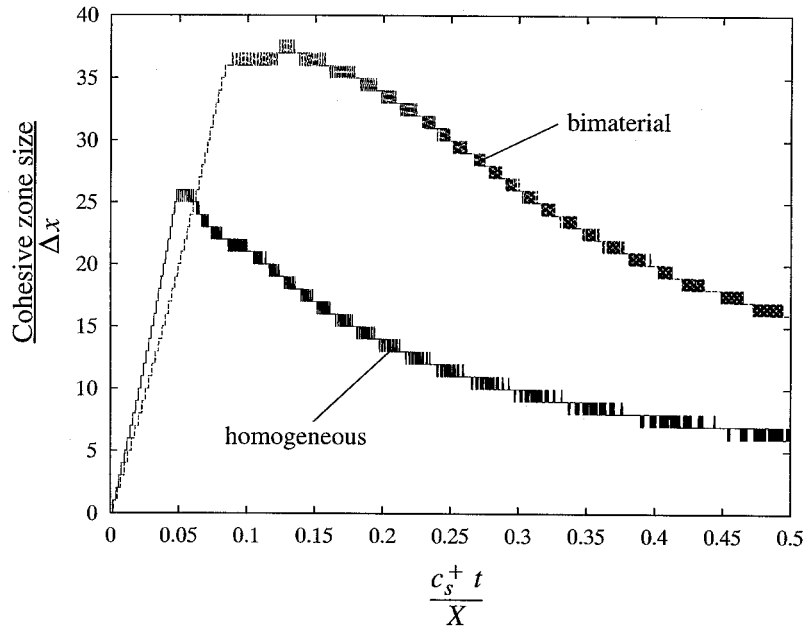


Figure 12. Evolution of the size of the cohesive zone in the homogeneous and bimaterial crack propagation problems, showing the rise associated with the initiation phase and the subsequent continuous decrease as the trailing edge of the cohesive zone (i.e., the crack tip) ‘catches up’ with the leading edge during the acceleration phase.

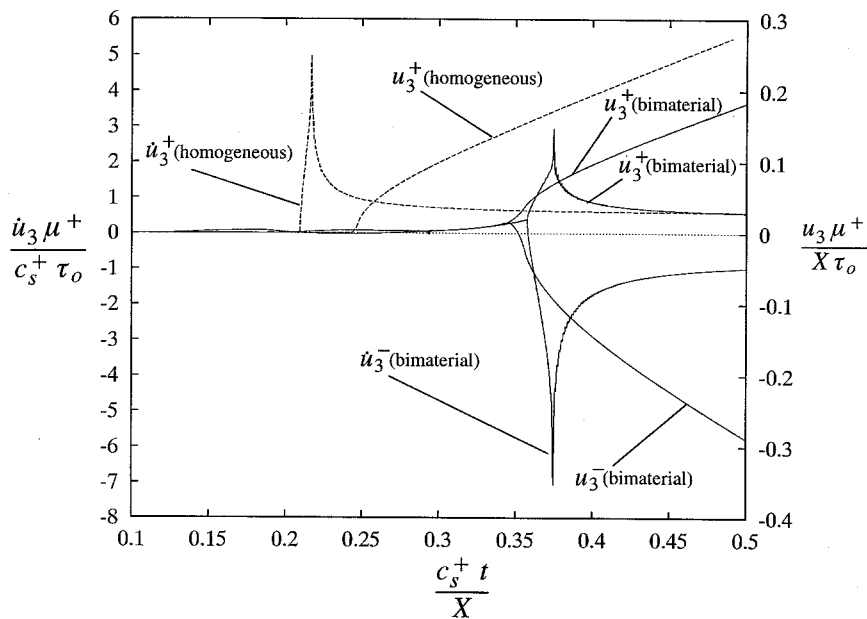


Figure 13. Evolution of the velocity and displacement of the crack surfaces observed at a point located  $X/8$  away from the initial right crack tip in the spontaneous crack propagation simulation presented in Figures 10 to 12.

fact is confirmed in this simple simulation, as the bimaterial static limit takes much longer to establish itself than its homogeneous counterpart.

The stress and displacement overshoot characteristic of most dynamic fracture problems, already apparent in Figure 5, can be quantified by extracting the dynamic stress intensity factor  $K_{\text{III}}(t)$  from the computed displacement discontinuity  $\delta(r, t)$  in the vicinity of the crack tips (Morrissey and Geubelle, 1997)

$$K_{\text{III}}(t) = \lim_{r \rightarrow 0} \sqrt{\frac{\pi}{2r}} \left( \frac{1}{\mu^+} + \frac{1}{\mu^-} \right)^{-1} \delta(r, t).$$

The evolution of  $K_{\text{III}}(t)$ , normalized by its static limit  $K_{\text{III}}(\infty) = \tau_0 \sqrt{\pi a}$ , is presented in Figure 6 in both the homogeneous and bimaterial cases. Note how the motion of the interface in the vicinity of the crack tip reduces the dynamic overshoot.

Finally, the motion of the interface is presented in Figure 7 for a point located at a distance  $a/8$  from the left crack tip. As expected, no motion is detected for the interface until the arrival of the fastest wave ( $c_s^+ t/2a = 0.5$ ) originated at the nearest crack tip and traveling along the stiffer material. The arrival of the first series of elastic waves is once again indicated by circled numbers.

#### 4. Fast debonding under anti-plane shear loading

As mentioned before, one of the most attractive aspects of the spectral scheme is its ability to simulate a wide range of phenomena associated with the *forced* (i.e., with imposed velocity) and *spontaneous* fast propagation of faults and cracks. In this section, simulations involving these two types of propagating mode III cracks are performed with the bimaterial spectral scheme.

Most of the analytical investigations of the structure of the near-tip field for a propagating interfacial cracks involve steady-state conditions, which can be simulated with the proposed spectral scheme by extending the crack at an *imposed* rate. If the spatial discretization is sufficiently refined, the inevitable transient effects associated with the step-like propagation of the crack along the discretized fracture plane can be minimized, as illustrated in this first example. In a recent paper, Yu and Yang (1994) showed that while the singularity  $p$  characterizing the near-tip bimaterial stress field ( $O(r^{-p})$ ) is constant ( $\rho = \frac{1}{2}$ ) in the subsonic regime, it depends on the crack velocity  $v_c$  in the transonic case ( $c_s^- < v_c < c_s^+$ ) as

$$p = \frac{1}{\pi} \tan^{-1} \left( \frac{\mu^+ \sqrt{(v_c/c_s^-)^2 - 1}}{\mu^- \sqrt{1 - (v_c/c_s^+)^2}} \right). \quad (19)$$

The singularity can be extracted numerically from the spatial variation of the slip behind the moving crack tip (Figure 8). A comparison between the analytical (19) and numerical values of the near-tip singularity is presented in Figure 9, showing good agreement throughout the crack velocity range, except when the imposed crack velocity approaches the higher shear wave speed, since steady-state conditions are then hard to achieve.

Finally, the issue of limiting *spontaneous* crack velocity under anti-plane shear conditions is examined with the aid of the proposed spectral scheme. As described by Atkinson (1977), the energy release rate of an interfacial crack subjected to mode III loading tends to zero as the crack velocity approaches the lower shear wave speed. Yu and Yang (1994) showed that, in the transonic regime, no energy flows into the moving crack tip, but is transferred through the interface from the stiffer (elliptic) material to the more compliant (hyperbolic) one. They

also showed that the debonding speed cannot exceed the higher shear wave speed as long as the flow of energy through the interface is to remain bounded.

The analytical conclusions described above have been obtained in the idealized context of a mode III interfacial mathematically sharp crack propagating in a linearly elastic bimaterial system at a *prescribed constant* velocity (i.e., regardless of the failure process leading to the creation of new surfaces along the interface). It might be of interest to determine how the incorporation of a cohesive failure model allowing for a completely *spontaneous* motion of the crack may affect these conclusions.

Brock and Achenbach (1973) have included a Dugdale cohesive failure model in their analysis of the subsonic propagation of a semi-infinite mode III interfacial crack subjected to an impacting step-like plane stress wave. However, as is the case in the vast majority of analytical investigations, the extension velocity of the yield zone was deduced *a posteriori* by first deriving the structure of the near-tip fields associated with an interfacial crack propagating at an arbitrary steady-state velocity. The unknown velocity was then determined such as to prevent the appearance of a stress singularity in the vicinity of the expanding cohesive zone.

The numerical scheme proposed in this paper allows us to *directly* extract the instantaneous crack velocity in more complex geometrical settings under steady-state or unsteady conditions. To investigate the limiting velocity of a spontaneously propagating mode III interfacial crack, a portion  $X$  of the fracture plane is discretized in 2048 spacings  $\Delta x$ . A small initial crack (of length  $128 \Delta x$ ) centered at  $X/2$  is suddenly loaded with a uniform stress equivalent to 90 percent of the strength of the interface. The cohesive model chosen to characterize the interfacial failure process is the aforementioned simple linear rate-independent law, with a critical crack opening displacement  $\delta_c = 0.03$ .

'Snapshots' of the deformed shape of the expanding crack are shown in Figure 10 for the homogeneous (dashed curves) and bimaterial (solid curves) cases. Due to symmetry, only the right side of the discretized domain ( $x \geq X/2$ ) is shown. Also, to improve the clarity of the figure, the displacement of the bottom surface is not presented in the homogeneous case and can be obtained by mirror symmetry of the upper surface about the interface plane. The asymmetry of the bimaterial case and the motion of the interface are obvious. Regarding the crack tip motion, due to the stress concentration building up in its vicinity, the leading edge of the cohesive zone starts to propagate outward, while the trailing edge of the yield (or Dugdale) zone (i.e., the physical crack tip) remains stationary until complete failure ( $\delta > \delta_c$ ) is achieved. The crack tip then 'jumps forward' and starts to catch up with the leading edge of the cohesive zone. Since a constantly increasing supply of energy is provided to the system by applying the uniform stress on the faces of the expanding crack, the tips of the yield zone and of the crack keep accelerating as indicated in Figure 11, which presents the evolution of the velocities of the crack tip (solid curves) and of the yield zone leading edge (dashed curves). The small-scale oscillations apparent in the various curves are associated with the numerical derivation process (since the velocities are extracted from crack tip position results) and with the aforementioned unsteady crack advance process.

Since the crack tip velocity exceeds most of the time that of the leading edge of the cohesive zone, the size of the Dugdale zone decreases monotonically. This trend is confirmed in Figure 12. Numerical experiments have shown that 15 elements are typically needed in the cohesive zone to accurately capture the failure process and render the simulation independent of the spacing size  $\Delta x$ . This requirement becomes a problem as the size of the yield zone continues to decrease, and is probably the cause of the increased unsteadiness observed for high crack speeds. Despite a continuous supply of energy to the system, the crack does exceed

the predicted limit of the slower wave speed ( $c_s^- = c_s^+/\sqrt{2}$  in the bimaterial case) at which the size of the cohesive zone and the energy flux to the crack tip vanish. The limiting speed obtained for a mode III interfacial crack *with cohesive zone* is thus the same as that predicted by Yu and Yang (1994) in their analysis of a mode III *mathematically sharp* crack propagating steadily along an interface.

The final figure (Figure 13) presents the evolution of the velocity and displacement of a point located at a distance  $X/8$  of the initial crack tip in the same spontaneous debonding simulation. Once again, for the homogeneous case (dashed line) only the motion of the top fracture surface is presented for clarity. The response of the homogeneous and bimaterial cases are fairly similar: both present a singularity in their velocity response as the crack tip (i.e., the trailing edge of the cohesive zone) reaches the point of observation. The velocity jump is however much stronger in the homogeneous case, due to the ‘damping effect’ associated with the motion of the interface initiated by the arrival of the fastest wave speed at  $c_s^+ t = X/8$ . This effect associated with the motion of the interface is similar to that observed in the dynamic overshoot characterized in Figure 6 by the maximum value of the dynamic stress intensity factor.

It is clear that the rate-independent linear cohesive model used in the simulation is very simple and that the spontaneous propagation behavior is expected to be different if, for example, the failure process is chosen to be dependent on the crack velocity. It is worth mentioning again at this point that the spectral scheme allows the incorporation of a very wide range of cohesive models through the general equation (16). The detailed investigation of a wider class of cohesive failure models is however beyond the scope of this paper.

## 5. Conclusion

A spectral scheme has been specially developed to investigate various dynamic bimaterial fracture problems under anti-plane shear conditions. The numerical method, based on an exact spectral representation of the elastodynamic equations in the two half spaces, has been shown to provide a very accurate description of the shear stress and out-of-plane displacement along the fracture plane, including in the vicinity of the crack tip where parameters such as the dynamic stress intensity factor and the steady-state singularity have been extracted. The spontaneous debonding process under anti-plane shear conditions has also been investigated using a simple linear cohesive model, showing a monotonic decrease of the cohesive zone length as the crack speed accelerates and approaches the slower shear wave speed.

## Acknowledgements

This paper has been written as part of M.S. Breitenfeld’s Master’s thesis work, supported partially by a grant from the Campus Research Board of the University of Illinois. Some of the larger simulations presented in this paper have been performed on the Power Challenge array available at the National Center for Supercomputing Applications.

## References

- Adams, G.G. (1995). Self-excited oscillations of two elastic half-spaces sliding with a constant coefficient of friction. *Journal of Applied Mechanics* **62**(4), 867–872.
- Andrews, D.J. and Ben-Zion, Y. (1997). Wrinkle-like slip pulse on a fault between different materials. *Journal of Geophysical Research* **102**, 553–571.

- Atkinson, C. (1977). Dynamic crack problems in dissimilar media. *Mechanics of Fracture 4: Elastodynamic Crack Problems*, (Edited by G.C. Sih), Noordhoff, Leyden, 213–248.
- Breitenfeld, M.S. and Geubelle, P.H. (1997). Numerical analysis of dynamic debonding under 2D in-plane and 3D loading. Submitted to *International Journal of Fracture*.
- Brock, L.M. and Achenbach, J.D. (1973). Extension of an interface flaw under the influence of transient waves. *International Journal of Solids and Structures* **9**, 53–68.
- Comninou, M. (1977). The interface crack. *Journal of Applied Mechanics* **44**, 631–636.
- Day, S.M. (1991). Numerical simulation of fault propagation with interface separation. *EOS Transactions of the American Geophysics Union* **72**, 486.
- Delale, F. and Erdogan, F. (1988). On the mechanical modeling of the interfacial region in bonded half planes. *Journal of Applied Mechanics* **55**, 317–324.
- Geubelle, P.H. (1995). Finite deformation effects in homogeneous and interfacial fracture. *International Journal of Solids and Structures* **32**(6/7), 1003–1016.
- Geubelle, P.H. and Rice, J.R. (1995). A spectral method for 3D elastodynamic fracture problems. *Journal of the Mechanics and Physics of Solids* **43**, 1791–1824.
- Knowles, J.K. and Sternberg, E. (1983). Large deformations near the tip of an interface crack between two neo-Hookean sheets. *Journal of Elasticity* **13**, 257–293.
- Lambros, J. and Rosakis, A.J. (1995). Shear dominated transonic interfacial crack growth in a bimaterial – I. Experimental observations. *Journal of the Mechanics and Physics of Solids* **43**(2), 169–188.
- Liu, C., Lambros, J. and Rosakis, A.J. (1993). Highly transient elastodynamic crack growth in a bimaterial interface: higher order asymptotic analysis and optical experiments. *Journal of the Mechanics and Physics of Solids* **41**(12), 1887–1954.
- Liu, C., Huang, Y. and Rosakis, A.J. (1995). Shear dominated transonic interfacial crack growth in a bimaterial – II. Asymptotic fields and favorable velocity regimes. *Journal of the Mechanics and Physics of Solids* **43**(2), 189–206.
- Lo, C.Y., Nakamura, T. and Kushner, A. (1994). Computational analysis of dynamic crack propagation along a bimaterial interface. *International Journal of Solids and Structure* **31**(2), 145–168.
- Morrissey, J.W. and Geubelle, P.H. (1997). A numerical scheme for mode III dynamic fracture problems. *International Journal for Numerical Methods in Engineering* **40**, 1181–1196.
- Perrin, G., Rice, J.R. and Zheng, G. (1994). Self-healing slip pulse on a frictional surface. *Journal of the Mechanics and Physics of Solids* **43**, 1461–1495.
- Rice, J.R. (1988). Elastic fracture mechanics concepts for interfacial cracks. *Journal of Applied Mechanics* **55**, 98–103.
- Tippur, H.V. and Rosakis, A.J. (1991). Quasi-static and dynamic crack growth along bimaterial interfaces: a note on crack-tip measurements using coherent gradient sensing. *Experimental Mechanics* **31**(3), 243–251.
- Williams, M.L. (1959). The stress around a fault or crack in dissimilar media. *Bulletin of the Seismological Society of America* **49**, 199–204.
- Xu, X.-P. and Needleman, A. (1995). Numerical simulations of dynamic interfacial crack growth allowing for crack growth away from the bond line. *International Journal of Fracture* **74**, 253–275.
- Xu, X.-P. and Needleman, A. (1996). Numerical simulations of dynamic crack growth along an interface. *International Journal of Fracture* **74**, 289–324.
- Yang, W., Suo, Z. and Shih, C.F. (1991). Mechanics of dynamic debonding. *Proceedings of the Royal Society (London)* **A433**, 679–697.
- Yu, H. and Yang, W. (1994). Mechanics of transonic debonding of a bimaterial interface: the anti-plane case. *Journal of the Mechanics and Physics of Solids* **42**(11), 1789–1802.
- Yu, H. and Yang, W. (1995). Mechanics of transonic debonding of a bimaterial interface: the in-plane case. *Journal of the Mechanics and Physics of Solids* **43**(2), 207–232.